Available online at www.sciencedirect.com
ScienceDirect
Journal of Solid State Chemistry 181 (2008) 30–36
JOURNAL OF SOLID STATE CHEMISTRY
www.elsevier.com/locate/jssc

The Heusler phases $LiRh_2Si$ and $LiRh_2Ge$: Synthesis, structure and properties

Mark S. Bailey[a], Qing'an Li[a], Emil B. Lobkovsky[b], D.G. Hinks[a], J.F. Mitchell[a,*]

[a]*Materials Science Division, Argonne National Laboratory, Argonne, IL 60439, USA*
[b]*Department of Chemistry and Chemical Biology, Cornell University, Ithaca, NY 14853, USA*

Received 30 July 2007; received in revised form 22 October 2007; accepted 27 October 2007
Available online 5 November 2007

Abstract

The isostructural Heusler phases $LiRh_2Si$ and $LiRh_2Ge$ have been synthesized from the elements and an excess of lithium at 1000 °C. Both materials adopt the $CuMn_2Al$ crystal structure, space group $Fm-3m$ (No. 225) with the room temperature lattice parameter $a = 5.747(1)$ Å [Vol = 189.866(1) Å^3] and $a = 5.847(1)$ Å [Vol = 199.88(6) Å^3] for $LiRh_2Si$ and $LiRh_2Ge$, respectively. X-ray analyses suggest mixed site occupancy of the form $Li_{1-x}Rh_2Si_{1+x}$ ($x<0.4$), but not for $LiRh_2Ge$. Both materials are diamagnetic, $\chi_{mol}(LiRh_2Si) = -6\times10^{-5}\,cm^3(mole)^{-1}$ and $\chi_{mol}(LiRh_2Ge) = -10\times10^{-5}\,cm^3(mole)^{-1}$ and metallic with room temperature resistivities of approximately 19 and 32 μΩ cm, respectively. These properties are consistent with the calculated electronic structure.

Keywords: Lithium flux; Heusler phase; Heusler alloys; Lithium rhodium silicide; Lithium rhodium germanide; Intermetallic

1. Introduction

$CuMn_2Al$, the prototypical Heusler phase, was reported in 1903 [1] and aroused interest as, in contrast to its elemental constituents, it was found to exhibit ferromagnetism. Subsequent research has shown that a wide variety of elements can combine in the Heusler phase crystal structure, giving rise to a wide variety of interesting or exotic physical properties. For example, Fe_2VAl [2] and the orthorhombically distorted UPd_2Sn [3] are heavy fermion materials and the compounds RPd_2Pb can exhibit superconductivity ($R = Y$ [4,5]), antiferromagnetism ($R = Gd$ [5]) or, in the case of $YbPd_2Sn$ and within a narrow temperature range, both superconductivity and antiferromagnetism [6,7].

In contrast to the complex physics exhibited by these materials, the crystal structure of Heusler phases is rather simple, consisting of a face-centered unit cell ($Fm-3m$) with occupation of the special positions, 4*a*, 4*b* and 8*c*. Removal, in an ordered fashion, of half of the 8*c* atoms gives rise to the half-Heusler structure type exemplified by the promising thermoelectric material HoPdSn [8] and by NiMnSb, a material predicted [9] and experimentally observed [10] to exhibit half-metallic ferromagnetism. In addition to NiMnSb, it has been suggested that full-Heusler materials such as $MnCo_2Si$ and $RuMn_2Si$ may also exhibit half-metallic ferromagnetism, albeit with much smaller minority-spin gaps than NiMnSb [11,12].

The majority of Heusler-type phases contain a main group element, a transition element and either a rare earth or another transition element. These materials are typically synthesized from arc melting or a self-flux technique, depending upon the nature of the main group element. For example, if tin, lead or other such low-melting element is a component of the system, a self-flux technique may be used; on the other hand, if the main group element has a high melting point, such as silicon or germanium, arc welding is more often used. In recent times, the power of the flux technique has become apparent both for growth of crystals suitable for new structure discovery and/or careful property measurement [13,14]. Lithium shares many properties with the traditional fluxing metals (e.g. tin) that suggest potential as a flux for new materials but, more

*Corresponding author. Fax: +1 630 252 7777.
E-mail address: mitchell@anl.gov (J.F. Mitchell).

0022-4596/$ - see front matter © 2007 Elsevier Inc. All rights reserved.
doi:10.1016/j.jssc.2007.10.030

interestingly, is also qualitatively different from these same metals in physical characteristics such as electronegativity and density. Indeed, lithium has been used very successfully for the growth of new nitrides [15] and materials such as $LiAg_2In$ [16], $LiNi_2Si$ [17], and Li_2CuGe [18] provide evidence of the potential of lithium to act as a self-flux for Heusler phases and similar materials.

We are interested in exploring the potential of lithium as a flux for a variety of new materials. Recently, we reported on $Li_2Rh_3B_2$ grown from a lithium flux [19], and in this paper we report on the synthesis and characterization of $LiRh_2Si$ and $LiRh_2Ge$, two diamagnetic metals that represent the first reported compounds in the lithium–rhodium–silicon and lithium–rhodium–germanium phase fields.

2. Experimental

$LiRh_2Si$ and $LiRh_2Ge$ were synthesized from a stoichiometric mix of rhodium and either silicon or germanium and an excess of lithium. Typical reactions were between 200 mg Li (pieces from rod, surface mechanically cleaned, 99.9% Alfa Aesar), 297 mg Rh (powder, 99.95%, Aesar) and 41 mg Si (powder, 99.9%, Atomergic Chemetals Co.) or 105 mg Ge (lumps, 99.9999 + %, Ventron Alfa products), providing an elemental ratio of 20 Li: 2 Rh: 1 Si/Ge. These reagents were handled inside an argon filled glove box and loaded into a niobium tube that was welded shut under flowing argon (99.999%, further purified by flowing over Ti metal at 800 °C using a Centorr Associates arc furnace) and subsequently sealed under vacuum in an evacuated fused silica sheath. The reaction tube was placed upright into a muffle furnace, heated to 1000 °C at 1–2 °C/min, held at temperature for approximately 60 h, then cooled to room temperature at 0.5 °C/min. The niobium tube was opened inside the glove box and placed in a long stainless steel tube. The excess lithium was removed in approximately 11 h via sublimation under dynamic vacuum (~5 mTorr) with a temperature gradient from 575 °C to room temperature.

Low temperature single-crystal X-ray diffraction of $LiRh_2Si$ (173 K) was performed with a Bruker Apex II Diffractometer. Data were collected and reduced with the SMART and SAINT-Plus software packages [20], respectively. An empirical absorption correction was applied with the program SADABS [21]. Room temperature single-crystal X-ray diffraction of $LiRh_2Si$ and $LiRh_2Ge$ were performed with a STOE IPDS IIT single-crystal X-ray diffractometer. Data were collected, reduced and corrected for absorption with the X-area suite of programs [22]. In both systems, data analysis were carried out with the SHELX [23] suite of programs and WinGX [24]. Room temperature powder X-ray diffraction analysis was carried out on a PANalytical X'Pert Pro MPD in Bragg-Brentano geometry with Co K_α radiation and an X'celerator detector. Samples were ground in an agate mortar inside an argon-filled glove box, loaded onto a greased sample slide and covered with Mylar film (0.00012″ thick) before being transported to the diffractometer.

Electron microprobe analysis was carried out on a Hitachi S-2700 SEM equipped with a light-element window Noran EDS detector. Samples of $LiRh_2Si$ and $LiRh_2Ge$ were selected under an optical microscope and loaded onto carbon tape for analysis.

A Quantum Design MPMS SQUID Magnetometer was used to measure the DC magnetization of a sintered pellet of $LiRh_2Si$ (146 mg, 0.606 mmol) and $LiRh_2Ge$ (160 mg, 0.561 mmol). The diameter of the pellets was well matched to the inside diameter of the straw used to suspend the sample inside the pick-up coils; therefore, the pellets could be loaded directly into the straw without the need for a gel cap or other sample holder. The samples were loaded into the straw inside argon filled glove box and transported to the SQUID in an argon atmosphere before being loaded into the sample space.

A DC four-probe resistivity measurement was performed on a single crystal of $LiRh_2Ge$ [$(0.1 \times 0.1 \times 0.3)$ mm^3] and a sintered cylindrical pellet of $LiRh_2Si$ (diameter 0.45 cm, height 0.25 cm). Four gold wires were attached to the samples with silver epoxy, which was cured (~160 °C, 10 min) in a nitrogen purged glove bag. Once the silver epoxy had cured, the crystal and contacts were encapsulated inside non-conducting, fast setting epoxy. Data were recorded at 2 s intervals on cooling.

The electronic structure of $LiRh_2Ge$ was calculated using its primitive cell ($a = 4.134$ Å, $\alpha = 60°$, $Z = 1$) at the extended Hückel level with the program YAeHMOP using Slater-type orbitals and default values of orbital energies and exponents [25]. Average properties were calculated using a set of 408 k points within the irreducible wedge of the first Brillouin zone.

3. Results and discussion

Crystals of $LiRh_2Si$ and $LiRh_2Ge$ are silver and grow with high symmetry habit, often as truncated cubes or octahedra. Samples of both phases were analyzed by single-crystal X-ray diffraction, and the initial structural model (Heusler phase, space group $Fm\bar{3}m$, no. 225) obtained via direct methods. This is the highest symmetry space group consistent with the experimental diffractograms and, as expected, no higher symmetry was found by ADDSYM [24]. The final refinement details for both $LiRh_2Si$ and $LiRh_2Ge$ are shown in Table 1. The atomic coordinates were standardized with STRUCTURE TIDY [26] and are listed, along with the isotropic displacement parameters, in Table 2. Important interatomic separations are shown in Table 3.

The refinement of $LiRh_2Ge$ converged smoothly to a stoichiometric compound whose composition is in good agreement with the ratio Rh/Ge = 1.8 ± 0.2 measured from SEM–EDS analysis; however, the optimum refinement of $LiRh_2Si$ required the lithium site (4*a*) to be of mixed lithium silicon occupancy (83% Li, 17% Si) giving a

Table 1
Crystal data and structure refinement for $LiRh_2Si$ and $LiRh_2Ge$

Empirical formula	$Li_{0.83}Rh_2Si_{1.17}$	$LiRh_2Ge$
Formula weight/ g(mol)$^{-1}$	244.39	285.35
Temperature/K	173(2)	Room temperature
Wavelength/Å	0.71073	0.71073
Crystal system, space group	Cubic, *Fm−3m*	Cubic, *Fm−3m*
a/Å; volume/Å^3	5.740(1); 189.159(17)	5.847(1); 199.88(7)
Z, ρ_{calc}/mg m^{-3}	4, 8.582	4, 9.482
μ/mm^{-1}	17.644	30.742
Crystal size/mm^3	(0.15 × 0.025 × 0.02)	(0.12 × 0.1 × 0.08)
θ range/°	6.16–40.04	6.04–37.43
Limiting indices	$-10\leqslant h\leqslant 7$, $-10\leqslant k\leqslant 6$, $-10\leqslant l\leqslant 5$	$-9\leqslant h\leqslant 10$, $-8\leqslant k\leqslant 8$, $-10\leqslant l\leqslant 10$
Reflections collected/unique	760/52 [Rint(0.0217)]	897/46 [Rint(0.0522)]
Completeness to θ_{max}	100%	100%
Absorption correction	Empirical	Integration
Max. and min. trans.	0.7192 and 0.1772	0.0702 and 0.0232
Data/restraints/ parameters	52/1/7	46/0/5
Goof on F^2	1.180	1.369
Final R indices $[I>2\sigma(I)]$	$R1 = 0.0121$, $wR2 = 0.0269$	$R1 = 0.0197$, $wR2 = 0.0481$
R indices (all data)	$R1 = 0.0145$, $wR2 = 0.0274$	$R1 = 0.0197$, $wR2 = 0.0481$
Largest diff. peak, hole/e Å^{-3}	+1.448, −0.830	+2.088, −1.060

Table 2
Atomic coordinates and isotropic displacement parameters (Å$^2 \times 10^3$) for $LiRh_2Si$ (at 173 K) and, in italics, $LiRh_2Ge$ (at room temperature)

Atom	Wyckoff	x	y	z	U_{iso}	Occ.
Li	4*a*	0	0	0	7 (2)	0.83(2)
Si	4*a*	0	0	0	7 (2)	0.17(2)
Si	4*b*	0.5	0.5	0.5	6 (1)	1
Rh	8*c*	0.25	0.25	0.25	4 (1)	1
Li	*4a*	0	0	0	*15 (10)*	*1*
Ge	*4b*	0.5	0.5	0.5	*9 (1)*	*1*
Rh	*8c*	0.25	0.25	0.25	*9 (1)*	*1*

The displacement parameters of the lithium and silicon atoms occupying the 4*a* site were fixed to be identical and the total occupancy of the 4*a* site was constrained to be 1. Anisotropic displacement parameters were not used for rhodium, silicon or germanium as their site symmetries preclude anisotropic motion.

stoichiometry $Li_{0.83}Rh_2Si_{1.17}$ (Rh/Si = 1.71). Refinements with the lithium occupancy of the 4*a* site fixed at 100% and with a reasonable but fixed isotropic displacement parameter yielded comparable R indices as in Table 1 but a very uneven Fourier difference map (+7, −1 eÅ^{-3}), indicating an incorrect model. As we discuss below, the small X-ray cross section of lithium makes it difficult to completely assign stoichiometry on the basis of X-ray data alone; however, it is certain that $LiRh_2Si$ and $LiRh_2Ge$ are two new Heusler-type materials. Further details of the crystal structure investigations are available from the Fachinformationszentrum Karlsruhe, D-76344 Eggenstein-Leopoldshafen (Germany) on quoting the depository numbers CSD-417738 ($LiRh_2Si$) and 417739 ($LiRh_2Ge$), the name of the authors and citation of this paper.

Table 3
Interatomic separations in $LiRh_2Si$ (left-hand side, 173 K) and $LiRh_2Ge$ (right-hand side, room temperature) less than 3 Å

Atoms	No.	Dist/Å	Atoms	No.	Dist/Å
Li–Rh	8	2.486(1)	Li–Rh	8	2.532(1)
Si–Rh	8	2.486(1)	Ge–Rh	8	2.532(1)
Rh–Rh	6	2.870(1)	Rh–Rh	6	2.923(1)
Li–Si	6	2.870(1)	Li–Ge	6	2.923(1)

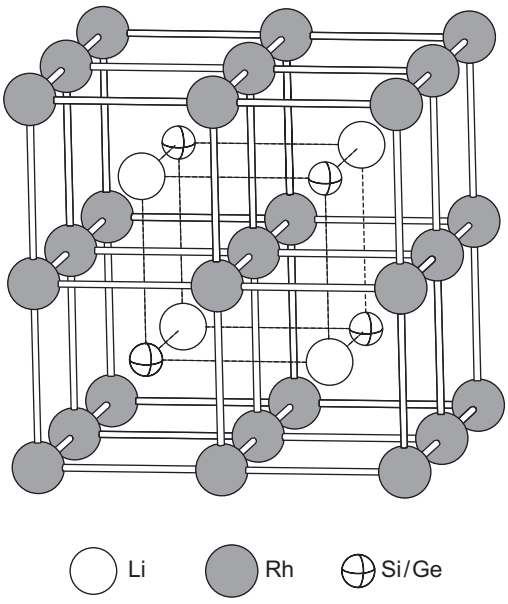

Fig. 1. The crystal structure of $LiRh_2Si$ and $LiRh_2$ Ge. The origin has been shifted by $(\frac{1}{4}, \frac{1}{4}, \frac{1}{4})$ to better illustrate the CsCl-type superstructure.

3.1. Stoichiometry of $LiRh_2Si$

The Heusler phase crystal structure adopted by $LiRh_2Si$ and $LiRh_2Ge$ shown in Fig. 1 derives from a specific patterning of an underlying bcc lattice and can be considered a superstructure of the CsCl structure type. There are a number of other structure types (such as the NaTl structure type) that can be formed by a different patterning of the bcc lattice [27] but, due to the excellent X-ray contrast afforded by lithium, rhodium and silicon/germanium, it is clear from our data that the parent structure is the Heusler-type phase shown in Fig. 1. However, due to the small X-ray cross section of lithium, we cannot definitively assign the degree or existence of the

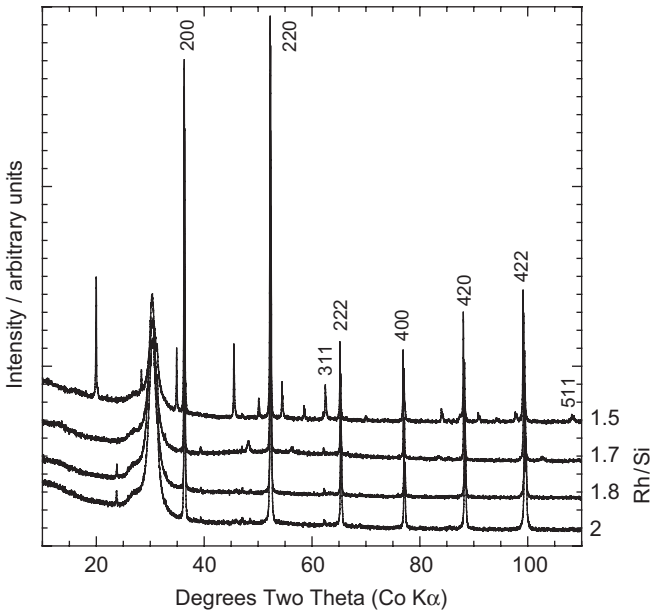

Fig. 2. The powder X-ray diffractograms from reaction with varying Rh/Si ratios. The 111 and 331 reflections are small but observed and indexed. We assign the peak at ~24° 2θ to LiOH, presumably introduced during the distillation step. The broad hump centered at ~30° 2θ is due to the Mylar cover.

non-stoichiometry of the form $Li_{1-x}Rh_2Si_{1+x}$ implied by the $LiRh_2Si$ single-crystal X-ray data [28].

To explore the potential variability of x in $Li_{1-x}Rh_2Si_{1+x}$, further reactions between excess lithium and varying ratios of Rh:Si were performed. As shown in Fig. 2, powder X-ray diffractograms of reactions with $1.7 < Rh/Si < 2.0$ were essentially identical, all containing peaks that could be indexed to a face centered cubic cell ($a = 5.755$ Å) and 2–3 impurity peaks whose intensities were $<1\%$ of the main $LiRh_2Si$ peak. It is normally expected that varying composition induces a varying lattice parameter (Vegard's law), but full-profile intensity extractions with the program FULLPROF [29] via the Le Bail method showed that the lattice parameters changed by $<0.5\%$ over the range of the attempted experiments, which may imply a single value of x in $Li_{1-x}Rh_2Si_{1+x}$. However, it is difficult to draw conclusions about from Vegard's law considerations alone as there is conflicting evidence in the literature concerning similar materials with structures based upon coloring of a bcc lattice; for example, Li_2PdSn and $LiPd_2Sn$ have identical lattice parameters [30]. On the other hand, materials of the form $Li(Ag_{1-x}In_x)_3$ do obey Vegard's law [16].

When the silicon concentration was increased further, to $Rh/Si = 1.5$, the impurity concentration increases dramatically: peaks corresponding to $LiRh_2Si$ are still evident in the powder X-ray diffractogram, but the intensity of the peaks that cannot be indexed to the $LiRh_2Si$ unit cell increases to ~20% of the main $LiRh_2Si$ peak [31]. Semi-quantitative SEM–EDS analysis of crystals with the same habit as those used in the single-crystal measurement revealed $Rh/Si = 1.9 \pm 0.3$. The large scatter in the ratio could reflect an intrinsic variation in stoichiometry between crystals or reflect varying geometry of the crystal facets with respect to the electron beam.

While we recognize the limitations of our X-ray-based analytical tools, the experiments detailed above do suggest that the material $Li_{1-x}Rh_2Si_{1+x}$ is non-stoichiometric, and that there is a limit to the non-stoichiometry, i.e. $x < 0.4$; however, we cannot be confident about the absolute value of x or if it can take a range of values. For clarity, the formula $LiRh_2Si$ will be used throughout the remainder of the paper, as the existence of the phase is not in doubt.

3.2. Structure description

As noted above, $LiRh_2Si$ and $LiRh_2Ge$ are isostructural and crystallize in the $MnCu_2Al$ structure type (full-Heusler phase) shown in Fig. 1. The structure is built from a certain atomic coloring of a bcc lattice that results in an array of primitive rhodium cubes centered either by lithium or silicon/germanium. The observed room-temperature rhodium–rhodium separations of 2.874(1) Å ($LiRh_2Si$, Le Bail extraction) and 2.923(1) Å ($LiRh_2Ge$, single crystal) are longer than the elemental rhodium–rhodium separation of 2.69 Å, suggesting that the rhodium–rhodium interaction is less significant in $LiRh_2Si$ and $LiRh_2Ge$ than in rhodium metal. The room-temperature lithium–rhodium and silicon/germanium–rhodium separations are necessarily identical and take values of 2.489(1) and 2.532(1) Å in $LiRh_2Si$ and $LiRh_2Ge$, respectively. These values are consistent with separations observed in RhSi [32] ($d_{Rh-Si} = 2.37$ Å), Rh_3Si_2 [33] ($d_{Rh-Si} = 2.44$ Å), and RhGe [34] ($d_{Ge-Rh} = 2.49$ Å). The Li–Rh separations in LiRh [35], $d_{Rh-Li} = 2.66$ Å, are longer than those observed in the title phases, suggesting that lithium is rather more ionic in $LiRh_2Si$ and $LiRh_2Ge$ than in the binary LiRh phase, a conclusion consistent with the electronic structure calculations shown below.

A number of Heusler phases of the form $LiTM_2Si$ (TM = Ni [17] and Cu [18]) and $LiTM_2Ge$ (TM = Co [36], Ni [17], Cu [18] and Pd [30]) have been reported. In addition to adopting the Heusler alloy structure, a number of elemental combinations also form more lithium rich phases; for example, both $LiPd_2Ge$ and Li_2PdGe have been reported with very similar lattice parameters, differing only in the patterning of the underlying CsCl superstructure [30]. Despite synthesizing both $LiRh_2Ge$ and $LiRh_2Si$ from a lithium rich melt, we did not see evidence in the intensity of the peaks from powder or single-crystal data for the formation of such a lithium rich phase in our limited exploration of the Li—Rh–Si and Li–Rh–Ge phase fields.

3.3. Electrical resistivity

The measured temperature dependence of the electrical resistivity of $LiRh_2Si$ and $LiRh_2Ge$ are shown in Fig. 3. The data for $LiRh_2Ge$ were obtained from a single crystal

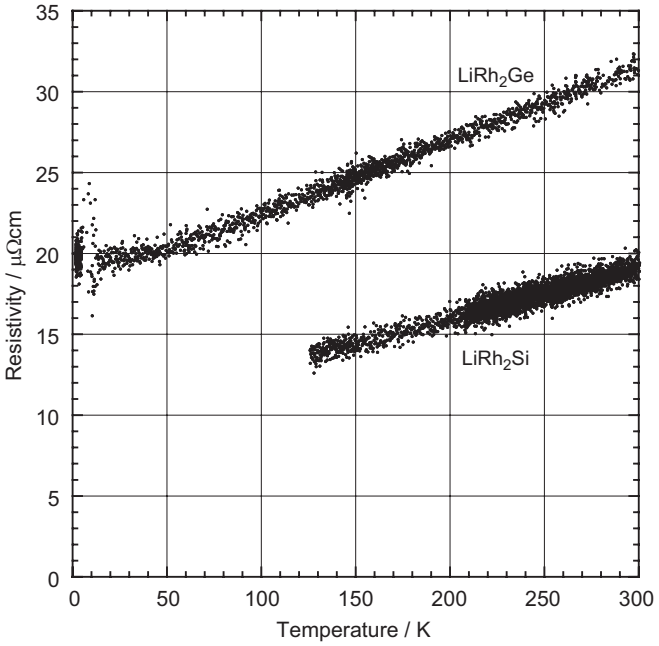

Fig. 3. The measured electrical resistivity of a single crystal of $LiRh_2Ge$ and a sintered pellet of $LiRh_2Si$. The noise in the data is due to the small voltage measured. The extra noise at $T<5$ K is due to temperature-induced contact fluctuations.

and we estimate an error of up to a factor of two in the absolute value of the resistivity, as the geometrical factor is not well described. The crystals of $LiRh_2Si$ were too small for four leads to be successfully mounted and the data shown are from a sintered pellet, and data were recorded only to 125 K as, below this temperature, the current path through the pellet abruptly changed. Extrinsic scattering events are always of concern when analyzing polycrystalline materials and the data presented for $LiRh_2Si$ in Fig. 3 represent an upper limit to the intrinsic resistivity of $LiRh_2Si$. Nevertheless, the slope of $d\rho/dT$ is positive for $LiRh_2Si$ and $LiRh_2Ge$, indicating metallic conductivity for both materials.

A linear dependence between the resistivity and temperature is typically observed for $T \gg \Theta_D$ [37], the Debye temperature. It can be seen that $d\rho/dT$ is linear to approximately 60 K for $LiRh_2Ge$ and <120 K for $LiRh_2Si$ which, if taken at face value, implies an unusually low Θ_D ($\sim$60 K) for both materials. However, it is not obvious from either the composition or the crystal structure why one should expect such a low value and what could cause the required low frequency oscillation. Indeed, considerably larger values of Θ_D have been estimated from heat capacity measurements for a number of Heusler phases: Θ_D of the superconducting materials YPd_2Sn, YPd_2Pb and YPd_2In are, respectively, 165, 198 and 260 K [4]. Effects such as antiparamagnons [38] and non-Fermi liquid behavior [39] have been invoked to rationalize T-linear resistivities in high-T_c superconductors and heavy fermion materials, respectively; however, the lack of an obvious magnetic degree of freedom in the present case makes such explanations unlikely. We note that the rather large residual resistivity and small value of $\rho(300\,K)/\rho(5\,K)$ could indicate that the observed temperature dependence of the resistivity simply reflects a high degree of disorder scattering. Further work is required to fully understand the data presented in Fig. 3.

3.4. Magnetic susceptibility

The measured magnetization of $LiRh_2Si$ and $LiRh_2Ge$ at 200, 250 and 300 K are shown in Fig. 4. At high applied fields, $H>5000$ or 20,000 Oe for $LiRh_2Si$ and $LiRh_2Ge$, respectively, the response is linear and diamagnetic; however, as is evident from the initial positive slope of dM/dH, both samples contain a small amount of a paramagnetic impurity. The effect of the paramagnetic impurity is more pronounced as the temperature is lowered, resulting in a larger region of applied field for which dM/dH is positive, and a shallower diamagnetic slope at high field. Although not shown, the measured temperature dependence of the magnetization shows a Curie—Weiss-type dependence.

An estimate of the molar magnetic susceptibility ($\chi_{mol} = M/H$) of $LiRh_2Si$ and $LiRh_2Ge$ was found by taking the slope of the M vs. H data of Fig. 3 at $H>20{,}00$ Oe at 300 K. The values so calculated are $\chi_{mol}(LiRh_2Si) = -6\times10^{-5}\,cm^3(\text{mole } LiRh_2Si)^{-1}$ and $\chi_{mol}(LiRh_2Ge) = -10\times10^{-5}\,cm^3(\text{mole } LiRh_2Ge)^{-1}$. As noted above, the magnetic susceptibility of the paramagnetic impurity follows a $1/T$ dependence; therefore, the data taken at 300 K provide the closest estimate of the intrinsic susceptibility of both $LiRh_2Si$ and $LiRh_2Ge$ but

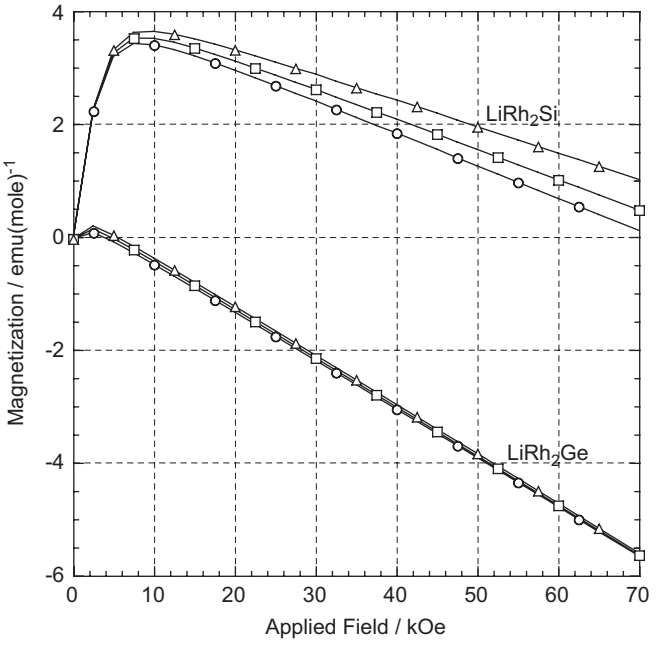

Fig. 4. The measured magnetization of $LiRh_2Si$ and $LiRh_2Ge$. Circles = 300 K, squares = 250 K and triangles = 200 K. Only $\frac{1}{6}$ of the data points are shown for clarity.

are only a lower limit on the absolute magnitude. Nevertheless, the small fraction of paramagnetic impurity present in the samples indicates that the error in the estimate is small; i.e., for both materials $|\chi_{mol}| > 10^{-5}\,cm^3(mole)^{-1}$, which is an order of magnitude larger than the related Heusler phases $LiCu_2Si$ and $LiCu_2Ge$, which have reported susceptibilities [18] of $-3\times10^{-6}\,cm^3(mole\ LiCu_2Si)^{-1}$ and $-4\times10^{-6}\,cm^3(mole\ LiCu_2Ge)^{-1}$.

3.5. Electronic structure calculations

The calculated density of states (DOS) of stoichiometric $LiRh_2Ge$ is shown in Fig. 5. The projected DOS of the rhodium and germanium are shown in Figs. 5a and b, respectively. The localized band centered at −18 eV derives mainly from the germanium 4*s* orbitals but contains a significant admixture of rhodium 4*d* and 5*p* character. The rhodium 4*d* orbitals are rather localized and filled, giving rise to the split peak centered at approximately −12.5 eV. Strong dispersion in the bands derived from the germanium 4*p* orbitals gives rise to the plateau in the DOS centered at approximately −7 eV but the character of the bands at the Fermi energy is a mixture of germanium 4*p* and rhodium 5*p* and 4*d*.

Although not shown, the calculated DOS of stoichiometric $LiRh_2Si$ is very similar to that shown in Fig. 5, the only difference arising from the greater radial extend of the silicon 3*s* orbital as compared to the more contracted germanium 4*s* orbital: the bandwidth of the lowest energy band is approximately doubled. Nevertheless, in both the calculated DOS shown in Fig. 5 and that of $LiRh_2Si$, the Fermi energy crosses through a finite DOS and is therefore consistent with metallic resistivity. The measured diamagnetism (Fig. 4) of $LiRh_2Ge$ and $LiRh_2Si$ suggests that core electrons contribute more to the overall magnetic susceptibility than the paramagnetic conduction electrons. As shown in Fig. 5, the bands deriving from the rhodium 4*d* orbitals are filled and rather localized, suggesting anionic d^{10} rhodium, which is consistent with the measured diamagnetism. As can be inferred from Fig. 5, there is no lithium character at or in the immediate vicinity of the Fermi energy, suggesting that the lithium is very ionic and, formally, it is possible to assign charges as $Li^+(Rh^-)_2Ge^+$,

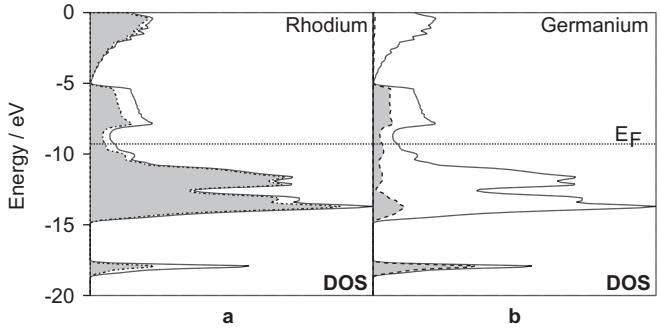

Fig. 5. The calculated DOS of stoichiometric $LiRh_2Ge$. Panels *a* and *b* contain the partial DOS of rhodium and germanium, respectively.

in reasonable agreement with the calculated average net charges of $Li^{+1}(Rh^{-0.8})_2Ge^{+0.6}$. We note that a similar effect was observed for $Li_2Rh_3B_2$, another diamagnetic metal containing formally closed shell rhodium and highly ionic lithium ions [19].

Based upon the above reasoning, it is possible to view the bonding in $LiRh_2Ge$ and $LiRh_2Si$ as an anionic, covalently bonded fluorite structure of rhodium and silicon/germanium with lithium cations providing charge-balance. This is in sharp contrast to the material $MnRh_2Ge$, in which the lithium atoms have been replaced by manganese, an element with considerable character in the vicinity of the Fermi level: $MnRh_2Ge$ is a ferromagnet ($T_c = 450$ K [40]) with localized spins residing upon the manganese atoms [11].

4. Conclusion

Building upon our recent report of $Li_2Rh_3B_2$, we have continued to demonstrate the viability of lithium as a flux for a variety of new materials. In this paper, we discuss our synthesis and characterization of the $LiRh_2Si$ and $LiRh_2Ge$, the first materials to be reported in their respective phase fields. We find both to exhibit metallic resistivity and diamagnetism that are consistent with the formalism, $Li^+(Rh^-)_2Si^+$ and $Li^+(Rh^-)_2Ge^+$.

Acknowledgments

We than John Schlueter for the use of the SQUID magnetometer and both Duck-Young Chung and Jens Richter for help with and use of the STOE single-crystal diffractometer. We also thank Ken Gray for discussions concerning the electrical resistivity. This work was supported by the US Department of Energy, Division of Basic Energy Sciences – Materials Sciences, under contract DE-AC02-06CH11357.

References

[1] F. Heusler, Verh. Dtsch. Phys. Ges. 76 (1903) 323.
[2] Y. Nishino, M. Kato, S. Asano, K. Soda, M. Hayasaki, U. Mizutani, Phys. Rev. Lett. 79 (1997) 1909–1912.
[3] C. Rossel, M.S. Torikachvili, J.W. Chen, M.B. Maple, Solid State Commun. 60 (1986) 563–567.
[4] M. Ishikawa, J-L. Jorda, A. Junod, in: W. Buckel, W. Weber (Eds.), Superconductivity in d & f Band metalsl, Kernforschungszentrum, Karlsruhe, 1982, pp. 141–144.
[5] C.L. Seaman, N.R. Dilley, M.C. de Andrade, J. Herrmann, M.B. Maple, Z. Fisk, Phys. Rev. B. 53 (1996) 2651–2657.
[6] H.A. Kierstead, B.D. Dunlap, S.K. Malik, A.M. Umarji, G.K. Shenoy, Phys. Rev. B 32 (1985) 135–138.
[7] A. Dönni, P. Fischer, F. Fauth, P. Convert, Y. Aoki, H. Sugawara, H. Sato, Physica B 259–261 (1999) 705–706.
[8] K. Mastronardi, D. Young, C.-C. Wang, P. Khalifah, R.J. Cava, A.P. Ramirez, Appl. Phys. Lett. 74 (1999) 1415–1417.
[9] R.A. de Groot, F.M. Mueller, P.G. van Engen, K.H.J. Buschow, Phys. Rev. Lett. 50 (1983) 2024–2027.
[10] K.E.H.M. Hanssen, P.E. Mijnarends, L.P.L.M. Rabou, K.H.J. Buschow, Phys. Rev. B 42 (1990) 1533–1540.

[11] I. Galanakis, P.H. Dederichs, N. Papanikolaou, Phys. Rev. B 66 (2002) 174429-1–174429-9.
[12] Y. Kurtulus, R. Dronskowski, G.D. Samolyuk, V.P. Antropov, Phys. Rev. B 71 (2005) 014425-1–014425-12.
[13] P.C. Canfield, Z. Fisk, Philos. Magn B 65 (1992) 1117–1123.
[14] M.G. Kanatzidis, R. Pöttgen, W. Jeitschko, Angew. Chem. Int. Ed. 44 (2005) 6996–7023.
[15] R. Niewa, F.J. DiSalvo, Chem. Mater. 10 (1998) 2733–2752; R. Niewa, H. Jacobs, Chem. Rev. 96 (1996) 2053–2062.
[16] V.V. Pavlyuk, G.S. Dmytriv, I.V. Chumak, H. Ehrenberg, H. Pauly, J. Solid State Chem. 178 (2005) 3303–3307.
[17] H.U. Schuster, A. Mewis, Z. Naturforsch. 24b (1969) 1190.
[18] H.U. Schuster, D. Thiedemann, H. Schönemann, Z. Anorg. Allg. Chem. 370 (1969) 160–170.
[19] M.S. Bailey, E.B. Lobkovsky, D.G. Hinks, H. Claus, Y.S. Hor, J.A. Schlueter, J.F. Mitchell, J. Solid State Chem. 180 (2007) 1333–1339.
[20] APEX2 (Version 1.22, 2004) and SAINT-Plus (Version 7.06a, 2003), Bruker Analytical Instruments, Inc. Madison, WI.
[21] G. M. Sheldrick, SADABS (Version 2.10) program for absorption correction, Bruker Analytical X-ray Instruments Inc., Madison, WI.
[22] X-RED Data Reduction for STADI4 and IPDS; Revision 1.22, March 2001 and X-Shape, X-Area version; Revision 2.03, October 2003. STOE & Cie GmbH, Darmstadt, Germany.
[23] G.M. Sheldrick, SHELX-97, Bruker Analytical Instruments Inc. Madison, WI.
[24] L.J. Farrugia, J. Appl. Crystallogr. 32 (1999) 837–838.
[25] G. Landrum, YAeHMOP (Version 3.0), 〈http://www.yaehmop.sourceforge.net〉
[26] L.M. Gelato, E. Parthé, J. Appl. Crystallogr. 20 (1987) 139–143.
[27] V.V. Pavlyuk, G.S. Dmytriv, I.V. Chumak, H. Ehrenberg, H. Pauly, J. Solid State Chem. 178 (2005) 3303–3307 For example, see discussion in.
[28] A second crystal was investigated by single crystal X-ray diffraction with comparable results; i.e., in order for a satisfactory refinement, the lithium site was of mixed lithium-silicon occupancy; in this case, $Li_{0.63}Rh_2Si_{1.37}$.
[29] J. Rodríguez-Carvajal, FULLPROF version January 2006, ILL (unpublished).
[30] C.-J. Kistrup, H.U. Schuster, Z. Anorg. Allg. Chem. 410 (1974) 113–120.
[31] We attempted to ascertain the identity of the impurity phase(s) but could not obtain a satisfactory indexing of the peaks or a matching solution from our databases.
[32] S. Bhan, K. Schubert, Z. Metallkd. 51 (1960) 327–339.
[33] L. Schellenberg, J.L. Jorda, J. Muller, J. Less-Common Met. 109 (1985) 261–274.
[34] S. Geller, Acta Crystallogr. 8 (1955) 15–21.
[35] S.S. Sidhu, K.D. Anderson, D.D. Zauberis, Acta Crystallogr. 18 (1965) 906–907.
[36] A. Mewis, H.U. Schuster, Z. Naturforsch. 26b (1971) 62.
[37] C. Kittel, Introduction to Solid State Physics, first ed., Wiley, New York, 1953.
[38] H. Monien, P. Monthoux, D. Pines, Phys. Rev. B 43 (1991) 275–287.
[39] J. Paglione, M.A. Tanatar, D.G. Hawthorn, E. Boaknin, R.W. Hill, F. Ronning, M. Sutherland, L. Taillefer, C. Petrovic, P.C. Canfield, Phys. Rev. Lett. 91 (2003) 246405-1–246405-4.
[40] F.A. Hames, J. Crangle, J. Appl. Phys. 42 (1971) 1336–1338.